Istraživanja i projektovanja za privredu
ISSN 1451-4117
DOI:10.5937/jaes0-71221
www.engineeringscience.rs

iipp publishing

Journal of Applied Engineering Science
Original Scientific Paper,
Volume 24, Number 4, Year 2026,
no 1372, pp 805-814

SCAN INDUCTION HARDENING OF S45C STEEL: THE EFFECT OF SCAN SPEED ON HARDNESS AND HARDENING DEPTH

Padang Yanuar[1,2]*, Sri Nugroho[1], Rifky Ismail[1], Rizal Mustofa[2], Yanuar Mahfudz Safarudin[3]

[1]Universitas Diponegoro, Faculty of Engineering, Department of Mechanical Engineering, Semarang, Indonesia
[2]Politeknik Negeri Semarang, Department of Mechanical Engineering, Semarang, Indonesia
[3]United Arab Emirates University, College of Engineering,
Department of Electrical and Communication Engineering, Al Ain, United Arab Emirates
**padang.yanuar@polines.ac.id*

This study aims to characterise the effect of scan speed on surface hardness and hardness distribution with depth in medium carbon steel S45C. The process is carried out using a static induction coil, while the workpiece with a diameter of 29 mm moves in both rotation and translation, followed by a quenching process. A total of 11 specimens were tested at a scan speed of 3.33-5.00 mm/s. Surface hardness was evaluated using the Rockwell C scale, while the hardness profile against depth was analysed using the Vickers method. The results show that the highest average hardness was obtained in Specimen 9 at 53.68 HRC at a speed of 3.66 mm/s, while Specimen 11 showed the best stability with an average of 53.00 HRC and a coefficient of variation of 4.27% at 3.53 mm/s. An increase in speed up to 4.69-5.00 mm/s tends to decrease surface hardness. The Vickers profile shows values of 544-637 HV in the near-surface area, then significantly decreases at a depth of about 1-2.5 mm and approaches 180-225 HV in the deeper sections. These results indicate the formation of a hardening gradient from the surface layer towards the transition zone and core. Overall, a scan speed of around 3.5-3.7 mm/s provides the best combination of hardness level, hardening response depth, and process stability in the experimental configuration used.

Keywords: hardening depth, induction hardening, S45C, scan speed, surface hardness

HIGHLIGHTS

- The IH scan speed affects the distribution of the material's surface hardness, with hardness values decreasing with increasing scan speed.
- A speed of 3.66 mm/s produced the highest average hardness along the shaft surface.
- A hardness gradient formed from the surface toward the core, with the highest hardness value at the surface and decreasing toward the core.
- The microstructure confirmed the hardness gradient, with martensite structure dominant at 1 mm from the surface.

1 Introduction

Energy efficiency is increasingly important in modern heat-treatment manufacturing, and induction hardening (IH) is attractive because electrical energy can be delivered rapidly and locally to the region that requires thermal treatment, thereby limiting unnecessary bulk heating and reducing prolonged furnace operation. Pfeifer et al. [1] showed that, for a press-hardening application, IH could reduce energy demand by up to 12% relative to furnace heating under continuous-production conditions, with the potential saving increasing to 19% when a 20% furnace standby share was considered. In the development of an IH system for steels, Stević et al. [2] reported energy efficiencies ranging from 75.3% to 95.1%, with approximately 90% occurring most frequently under the investigated conditions. Although these quantitative values are specific to their respective systems, they collectively demonstrate the potential of IH as an energy-efficient heat-treatment technology because heating is rapid, electrically driven, spatially localized, and readily interrupted when heating is not required. These characteristics make IH particularly relevant to advanced and sustainable manufacturing, while the metallurgical effectiveness of the treated layer must still be verified for each process configuration.

Enhancing the mechanical properties and surface characteristics of steel components can be achieved through various heat treatment and surface modification methods. Kombayev et al. [3] employed electrolytic-plasma hardening to improve the surface hardness and wear resistance of corrosion-resistant steel components, while Al-Saraireh and Suhymat [4] demonstrated that gas nitriding can increase the surface microhardness of high-speed steel cutting tools. These methods indicate that improvements to the surface properties of steel components can be realized by applying surface treatment technologies tailored to specific material characteristics and application requirements. IH is a surface heat treatment process used to enhance the surface and subsurface characteristics of steel components. Areitioaurtena et al. [5] explain that this process produces a hardened case that influences the component's surface and structural quality. In scanning IH research, several parameters are used to evaluate the material layer: hardness, microstructure, and residual stress distribution. Holmberg et al. [6] also report that progressive IH of C45E steel produces a martensitic layer with a transition zone leading to the base material. Thus,

process evaluation is relevant not only to surface hardness values but also to the characteristics of the hardened layer and the transition region.

In the progressive IH method, heating is achieved through relative movement between the inductor and the workpiece along the area to be hardened. Holmberg et al. [6] applied progressive IH to C45E steel using two scanning speeds: 5 mm/s and 27.5 mm/s. The study results indicated that varying the scanning speed led to differences in subsurface residual stress conditions, even though the conditions employed still met specific requirements regarding surface hardness, case depth, and microstructure. Under the faster scanning condition, the peak subsurface tensile residual stress was reported to be approximately twice as high as that observed under the slower scanning condition. These findings demonstrate that scanning speed is a process parameter that must be recorded and controlled when evaluating progressive IH experimentally. Šapek et al. [7] reported on the relationship between movement speed and hardening depth during the IH of work rolls made from tool-grade steel. Different feed rates of 24, 30, 36, and 42 mm/min can result in changes to hardening depth, microstructure, and wear characteristics. Reducing the feed rate from 36 to 24 mm/min increased the hardened layer depth from 16 to 25 mm, an increase of 56.25%. Although the material type, dimensions, and process configuration differed from those in the present study, the results provide experimental evidence that the speed at which the workpiece moves through the inductor correlates with the resulting hardening depth.

The influence of scanning speed was also reported by Saputro et al. [8] regarding the mobile IH of SCM440 gears. Their study evaluated the interactions between flank length, scanning speed, and air gap through experimental testing and numerical modelling. Processing temperature is also linked to metallurgical response during hardening. Li et al. [9] demonstrated that the heating temperature during the progressive IH of 55CrMo steel influences austenitization, microstructure, austenite grain size, tensile strength, and the stress state. Excessive heating temperatures in their setup were reported to cause grain growth and metallurgical issues that compromised hardening quality. Sun et al. [10] also reported on the effect of induction quenching temperature on the mechanical properties and microstructural evolution of 45 steel. However, the optimum temperatures identified in these studies are specific to the respective materials and processing conditions; therefore, they cannot be directly applied as reference values for the present experiment.

In addition to process parameters, initial microstructural conditions can influence material response during rapid IH. Seo et al. [11] studied rapid induction heating and hardening of medium carbon steel 1045 and found that the ferrite fraction and size in the initial microstructure influenced the austenitization process. Hardened layer depth is one of the parameters used to evaluate the results of the IH process. Holmberg et al. [12] performed IH on C45 steel to produce various hardening depths and evaluated their relationship with microstructure and Barkhausen signals. Destructive verification of material characteristics served as a reference for the development of this method. Areitioaurtena et al. [5] also compared hardness, microstructure, and residual stress profiles obtained from simulations with experimental data from scanning IH. Both studies support the use of hardness profiles and layer depths as parameters for characterizing process outcomes.

The aforementioned studies utilize controlled motion mechanisms to maintain a constant scan speed throughout the IH process. Existing data indicate a consistent material response to scan speed under these conditions. In contrast, IH scanning systems employing manual translation mechanisms have received limited attention. Manual scanning carries the risk of speed fluctuations during a single test stroke, potentially compromising the effectiveness of the induction hardening process. This study addresses this gap by characterizing S45C carbon steel subjected to manual scanning, utilizing a static induction coil configuration while the workpiece undergoes both rotational and translational movement. The evaluation focuses on directly observable parameters: scan speed, coil geometry, coupling distance, quenching conditions, surface hardness, and hardened layer characteristics. The study's novelty lies in its characterization of manual-translation induction hardening, specifically by correlating measured scan speeds with surface hardness and hardening depth profiles.

2 Materials and methods

2.1 Materials and workpieces

The workpiece used in this study is S45C medium carbon steel, this steel is widely used as an industrial component and possesses mechanical properties that can be enhanced through heat treatment [13, 14] . The specimens are shaft-shaped, with a diameter of 29 mm and a length of 310 mm. The chemical composition of the material is presented in Table 1. The initial material has a hardness value of 180 HB. The specimens underwent a turning process to clean the outer cylindrical surface, and their microstructure was examined using an optical microscope. Characterizing the initial material condition is necessary because Seo et al. [11] demonstrated that the ferrite fraction and size in the initial structure of 1045 steel can influence the austenitization response during rapid IH.

Table 1. Chemical composition of S45C workpiece material

Chemical composition (wt. %)							
C	Si	Mn	P	S	Cr	Ni	Mo
0.46	0.25	0.65	0.010	0.013	0.02	0.008	0.15

2.2 Scan induction hardening system

Experiments were conducted using high-frequency IH equipment with a power rating of 120 kVA. The induction coil remained stationary, while the workpiece was mounted on a mechanism capable of simultaneous rotational and translational movement. After the workpiece passes through the heating zone, its surface is quenched using water via a spray system, as shown in Figure 1. The coil was fabricated from copper tubing, with its geometric configuration summarized in Table 2. Research by Saputro et al. [8] indicates that the air gap, scanning speed, and flank length influence the hardening quality in mobile IH configurations.

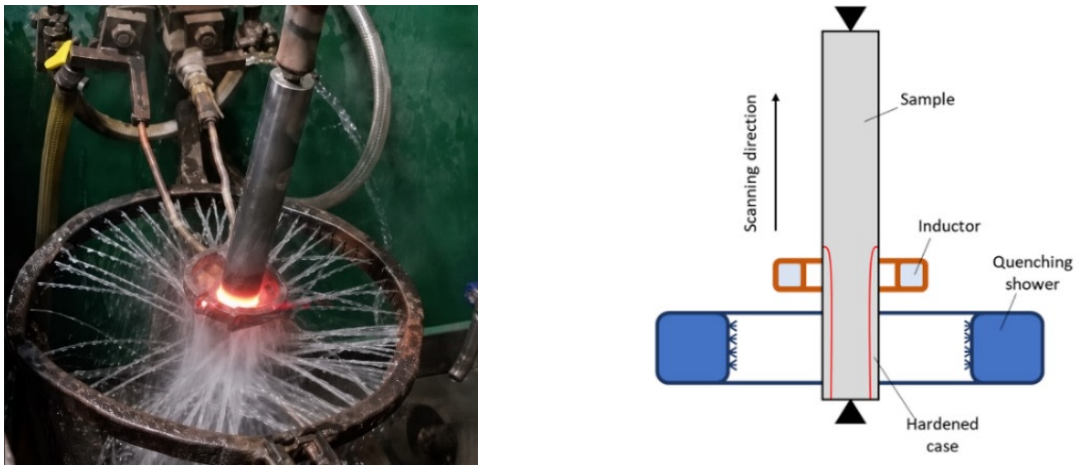

(a) (b)

Fig. 1. Scan IH process; (a) experiment; (b) graphical representation and key components

Table 2. Experimental process parameters

Parameters	Value
Number of turns	1
Inner diameter of the coil	69 mm
Workpiece coil distance	20 mm
Coil shape	solenoid coil
Coil material	copper
Fequency	High frequency
Power	120 kVA
Rotational speed of the workpiece	120 rpm
Quenching	water spray, immediately after the heating zone

2.3 Rotational-translational motion mechanism

During the hardening process, the workpiece undergoes translational movement past the coil while simultaneously rotating about its axis. The translation mechanism advances only while the operator holds the actuating button, so the axial motion consists of alternating displacement and dwell intervals rather than a continuous feed. The average scanning speed was obtained as vs = Ls/ts, where Ls is the total axial displacement (300 mm) and ts the total elapsed time of the run. The limitation of this method is the unavailability of real-time scanning speed measurement tools during the experiment. The use of scanning speed as an evaluation variable is supported by Holmberg et al. [6], who compared two scanning speeds in progressive IH, and Šapek et al. [7], who demonstrated changes in hardening depth resulting from variations in feed rate. In this study, kinematic measurements were conducted to capture the actual operating conditions of the manual system, enabling the analysis of the relationship between movement and hardening response based on experimental data.

2.4 Surface hardness testing

Surface hardness testing was conducted along the shaft to evaluate the hardness uniformity resulting from the scanning IH process. As shown in Figure 2, twenty measurement points were positioned along a longitudinal line on the shaft's outer cylindrical surface. This measurement arrangement was selected to obtain a representative hardness profile across the hardened zone. Surface hardness testing of IH parts is conducted using the ASTM E18 or Rockwell C (HRC) standard. The hardness values obtained at these points were then used to evaluate the axial

hardness distribution, calculate the average hardness and its variation for each specimen, and analyze the relationship between scanning speed and the uniformity of the surface hardness achieved through IH.

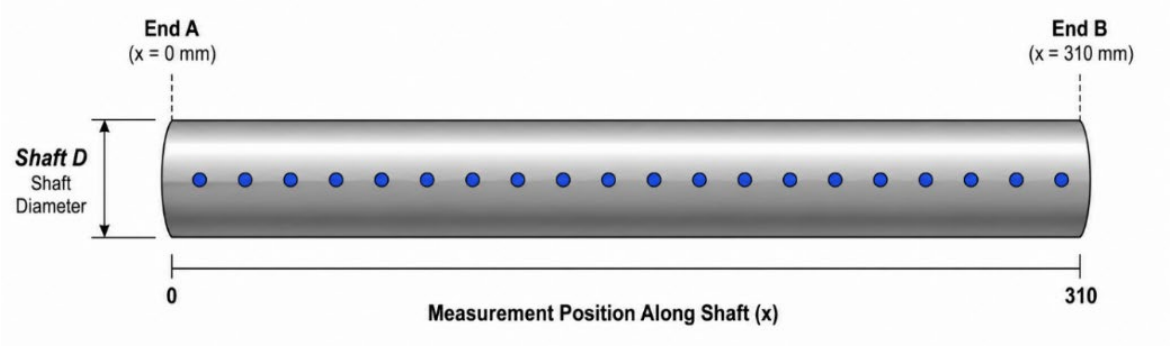

Fig. 2. Surface hardness testing method for the shaft

2.5 Hardening depth testing

The Vickers hardness method is employed to measure hardening depth and evaluate the effectiveness of IH, as surface hardness alone does not adequately characterize the depth of the zone undergoing hardening transformation. Hardness profiles extending from the surface to the core allow for the identification of the hardened zone, the transition zone, and the core material [15]. Choi & Lee [16] demonstrated the use of micro-Vickers measurements to validate the hardened zones resulting from the induction heat treatment of AISI 1045 steel. Consequently, hardening depth serves as a crucial parameter for correlating induction heating process conditions with the material's actual hardening response.

2.6 Microstructure Evolution

Metallographic observation was conducted on the cross-section of the hardened workpiece [17]. Samples were prepared through cutting, sanding, polishing, and etching. Observations are directed to compare the near-surface layer (1), the transition region (2), and the core material (3) as seen in Figure 3. Phase interpretation is only conducted based on actual observation results. The relationship between the initial microstructure condition and the results of IH will also be used to discuss its correlation with changes in hardness values.

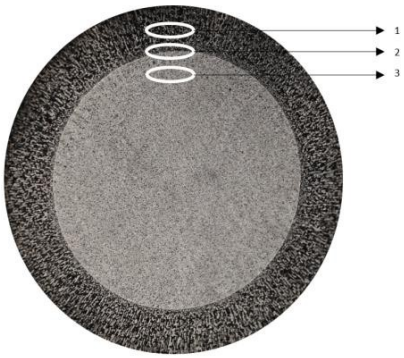

Fig. 3. The evolution of microstructure from the outer surface to the center surface

3 Results and discussion

3.1 Surface hardness distribution

Table 3 presents the changes in the workpiece's axial position over time during the IH scanning process. With a constant scan length of 300 mm, process times ranging from 60 to 90 seconds resulted in average scanning speeds between 3.33 and 5.00 mm/s, the measurement results can be seen in Table 4. This variation arose because the translational speed of the test specimen was manually controlled by the operator. Assessments regarding the stability or instability of the motion must be based on actual measurements of position and speed changes. The scanning speed influences the hardness values obtained from IH [6].

Table 3. Hardness test results

No	Surface Hardnes HRC										
	Spc 1	Spc 2	Spc 3	Spc 4	Spc 5	Spc 6	Spc 7	Spc 8	Spc 9	Spc 10	Spc 11
1	20,5	20	42,5	48	52	51	46	48	46	34	56
2	50	47	56	55	52	24	52	51	56	24	56

No	Surface Hardnes HRC										
	Spc 1	Spc 2	Spc 3	Spc 4	Spc 5	Spc 6	Spc 7	Spc 8	Spc 9	Spc 10	Spc 11
3	38	41	51	39,5	50,5	38,5	46,5	44	52,5	22	51
4	39	36	58	58	52	33	47	46	52	49	51
5	40	36	53,5	51,5	53	49,5	46,5	47	53,5	44	50
6	35	40	54	51	51,5	47	45,5	47	56,5	55	52,5
7	30	37	51	49	53	49	50,5	44	56	48	55,5
8	37	43,5	49	49	53	50	43	44,5	52,5	55,5	55,5
9	39	43,5	49	45	53,5	50,5	48,5	46,5	54	56	51,5
10	34	38	47	44	53	41	48	41	55	50,5	51
11	42,5	42,5	53	51	54,5	55	51,5	53	55,5	49	52,5
12	26,5	41	47	52	56,5	48	53	55	56,5	45,5	56
13	19	44	48,5	56	53,5	53,5	52	54	54,5	51	54
14	20	42	54,5	54	55	55	54	55,5	54	48	51,5
15	39	44	50,5	53	54,5	56	56	51,5	53,5	47	51,5
16	41	43	50	44	52	57	53	53,5	55	50,5	55
17	47	39	51	56	56	54	53	54,5	56	52	53,5
18	28,5	44	50	56	50	53	51,5	55	56	51,5	55,5
19	22	44	50,5	46	45,5	50	48,5	50,5	52,5	48	49
20	50	49,5	49,5	43,5	48,5	52,5	49,5	50	46	49	51,5

The 20-point surface hardness testing method for the test specimens (Figure 2) yielded average surface hardness values ranging from 34.90 to 53.68 HRC for each specimen, as shown in Table 1 and Figure 3. A negative linear relationship was observed between scan speed and mean surface hardness, expressed $HRC_{mean} = - 8.1179v_{scan} + 79.519$, with $R^2=0.5892$. Indicates that there is a 41.08% variation in surface hardness which is not only explained by the scanning speed factor, there is the influence of other process parameters such as heat energy density, cooling rate and cooling media. Manual scanning can also cause operator variability effects that affect the stability of the scan (difficult to maintain constant) thus causing local variations on each specimen surface. Physically, increasing the scan speed shortens the duration of the material's local exposure to the induction field, thereby reducing the thermal energy accumulated at each axial position. This condition can limit the degree of austenitization prior to quenching, ultimately resulting in reduced martensite formation and lower surface hardness. Beyond changes in average values, specimens processed at high scan speeds also exhibited greater axial hardness variation, as evidenced by coefficients of variation of 27.68% for specimen 1 and 20.75% for specimen 2.

The surface hardness distribution of specimens 1-11 (see Table 3) shows several points with low hardness values. These values occurred in specimens 1, 2, 6, and 10. This was influenced by the manual heating scan performed by the operator, resulting in several points with very low hardness values. For example, specimen 1 at point 13 had a hardness value of 19 HRC, specimen 2 at point 1 had a hardness value of 20 HRC, specimen 6 at point 2 had a hardness value of 24 HRC, and specimen 10 at point 3 had a hardness value of 22 HRC. These values occurred because the operator ran the induction coil too quickly during the scan at these points.

Table 4 then presents the relationship between scanning speed and average hardness. According to the SAE-J423 standard, effective case depth hardness is ≥45 HRC. Nine specimens had an average hardness value of ≥45 HRC, and two specimens had an average hardness value of ≤45 HRC. Specimens 1 and 2 have hardness values ≤45 HRC, because they have speeds of 4.69 and 5.00 mm/s, respectively. High scanning speeds can affect the hardness results of induction hardening.

Table 4. Relationship between scanning speed and average hardness

Specimen	Time (s)	Scan speed* (mm/s)	Mean HRC	SD	Median	Min–Max HRC	CV (%)
1	64	4.69	34.90	9.66	37.50	19.0–50.0	27.68
2	60	5.00	40.15	8.33	42.25	20–49.5	20.75
3	71	4.23	50.78	3.46	50.50	42.5–58.0	6.82

Specimen	Time (s)	Scan speed* (mm/s)	Mean HRC	SD	Median	Min–Max HRC	CV (%)
4	87	3.45	50.08	5.14	51.00	39.5–58.0	10.26
5	80	3.75	52.48	2.54	53.00	45.5–56.5	4.84
6	78	3.85	48.38	8.33	50.25	24.0–57.0	17.23
7	86	3.49	49.78	3.39	50.00	43.0–56.0	6.81
8	90	3.33	49.58	4.42	50.25	41.0–55.5	8.92
9	82	3.66	53.68	2.99	54.25	46.0–56.5	5.58
10	84	3.57	46.48	9.31	49.00	22.0–56.0	20.03
11	85	3.53	53.00	2.27	52.50	49.0–56.0	4.27
Note: Obtained from the length of the shaft divided by the time							

3.2 Hardness depth

The distribution of Vickers hardness relative to hardening depth is illustrated in Figure 5. The results indicate that all specimens exhibited a similar trend, with peak hardness values occurring near the surface (0-1 mm) and decreasing as depth increased. Surface hardness is in the range of 446-637 HV before significantly decreasing at a depth of 1-2.5 mm. At deeper sections or above 2.5 mm from the surface, hardness reaches the range of ±180-225 HV. This pattern indicates the formation of a hard layer gradient towards the transition area and then the core section that is unaffected by IH.

High surface hardness can be attributed to rapid heating and cooling, resulting in a microstructure dominated by martensite. This can also be attributed to the characteristics of the IH tool used, namely high-frequency IH, which can produce a hardening depth of 0.015 – 0.045 inches [18]. On the other hand, the decrease in hardness with depth indicates a reduction in the martensite fraction and an increase in ferrite and pearlite. Nakasone et al. [19] showed a similar pattern in the S45C shaft heated by IH. The hard region consists of martensite, the transition region consists of ferrite and martensite, and the core section consists of ferrite and pearlite. They also found that the ferrite fraction increases with surface depth. Furthermore, these findings are consistent with the research conducted by Holmberg et al. [6] on C45E, which shows that the transition zone towards the ferrite-pearlite base follows the martensite layer produced by IH. Microstructural changes are also directly related to the decrease in hardness profile with depth. Overall, this profile shows that the IH process results in hardening concentrated on the surface layer while the core maintains relatively low hardness. This is a desirable situation to produce a combination of a hard surface and a more ductile core.

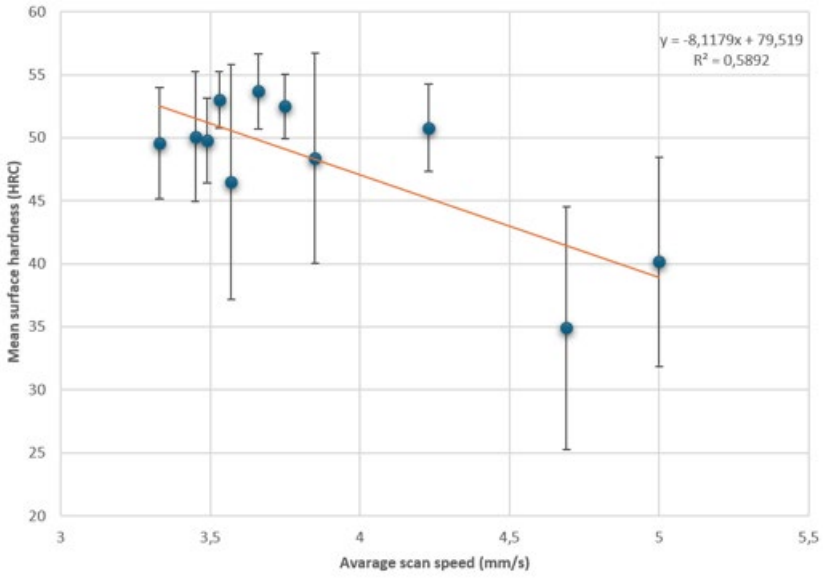

Fig. 4. Relationship between scan speed and mean surface hardness

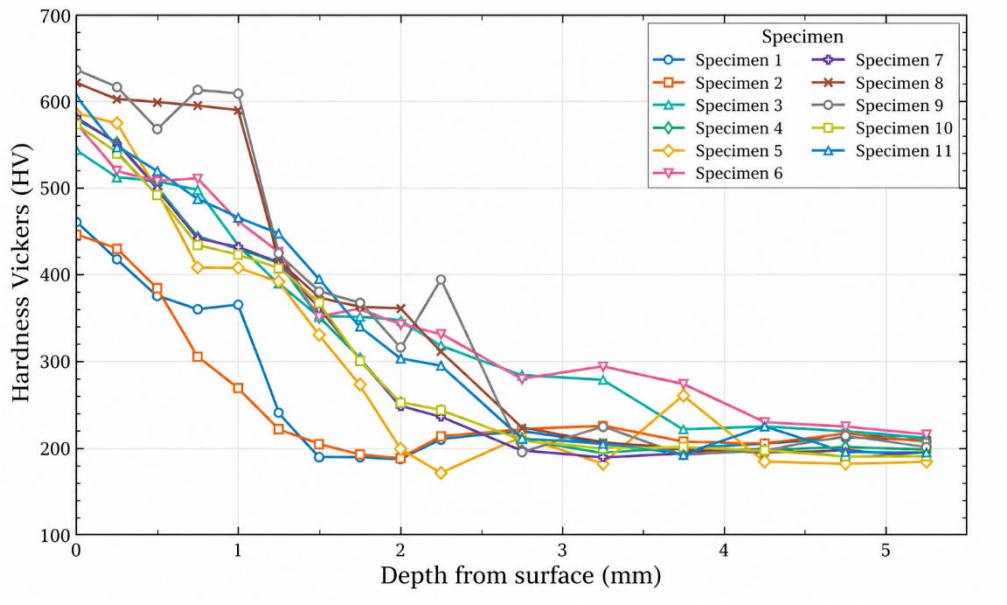

Fig. 5. Vickers hardness profiles as a function of depth from the surface

3.3 Microstructure evolution

Metallographic observation was carried out on the cross-section of Specimen 9, processed at a scanning speed of 3.66 mm/s. The micrographs in Figure 7 (a), (b) and (c) were taken at depths of 1 mm, 1.5 mm and 4 mm from the outer surface of that cross-section, so that the observed phases can be compared directly with the hardness values measured at the same depths. Figure 6 shows the initial microstructure of medium carbon steel S45C at 200X magnification. The microstructure is dominated by two main components: ferrite, which appears as bright areas, and pearlite, which is dispersed among the ferrite matrix. This morphology is a common characteristic of medium carbon steel in its initial condition before hardening [19]. While pearlite increases the strength and hardness of the material, ferrite makes its character softer and more ductile. The results of this study are consistent with Gao et al. [20] who state that the initial microstructure of AISI 1045 consists of ferrite (the lighter phase) and pearlite (the darker phase). This ferrite-pearlite structure is the initial structure that undergoes austenitization and microstructural changes during the IH process.

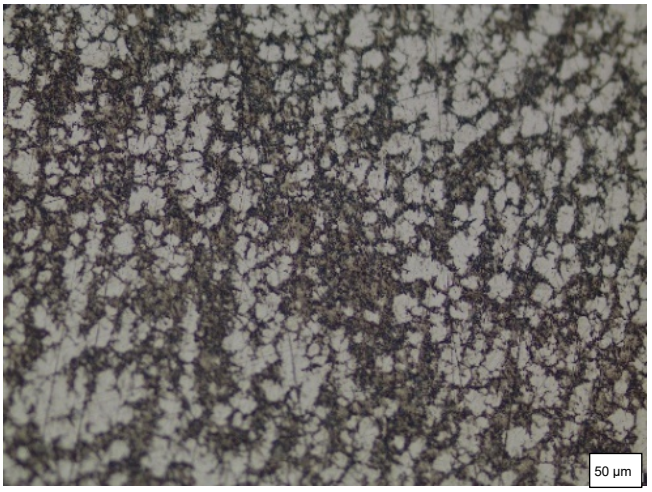

Fig. 6. Microstructure of S45C material in its initial condition before hardening at 200X magnification

Figure 7 shows the results of microstructural observations made on specimen 9. Figure 7(a) shows the microstructure obtained in the measurement area 1 mm from the outer side of the shaft, where the martensitic microstructure is visible. This location is near the surface that receives the most intense IH, followed by quenching. This area can be interpreted as the hardened region with a dominant martensitic structure. Gao et al. [20] also found that the hardened region in medium carbon steel AISI 1045 after IH is primarily composed of martensite but may still contain pearlite. Figure 7(b), measured 1.5 mm from the outer side, there is a transition area that appears as a mixture of dark and lighter regions. The lighter region (bottom left) consists of a combination of martensite and pearlite. Meanwhile, Figure 7(c), measured 4 mm from the outer side, a structure with a white/light colour can be identified as ferrite, while the dark region is pearlite structure. This indicates that IH heat does not reach the core, and the core structure essentially still retains the initial S45C structure.

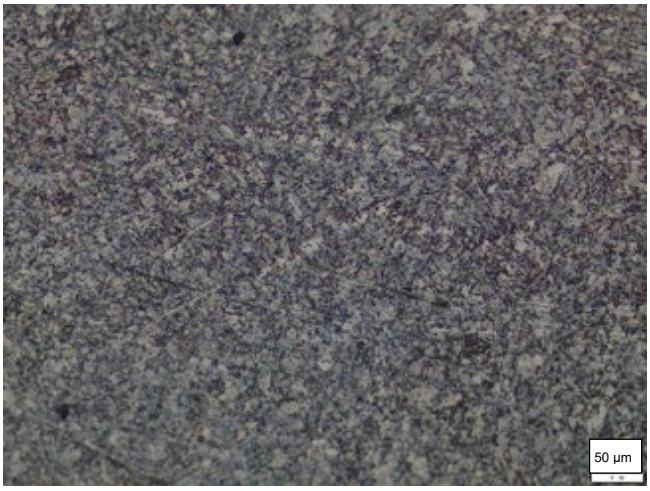

(a)



(b)

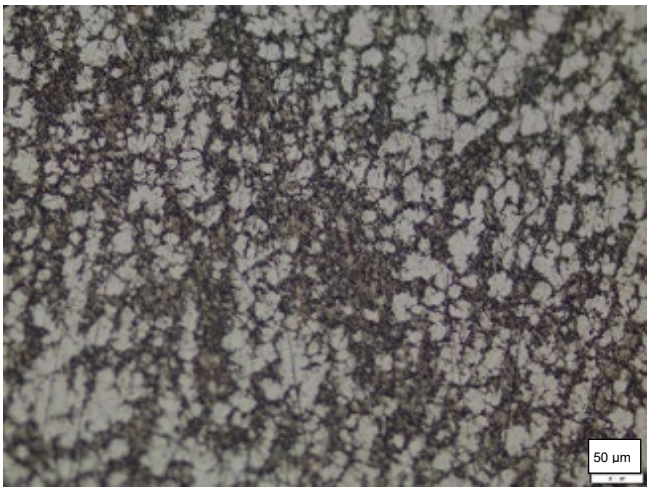

(c)

Fig. 7. Microstructure evolution of the IH from the outer diameter to the center of the specimen at 200X magnification; (a) measured 1 mm from the outside of the shaft, martensitic is visible; (b) measured 1.5 mm from the outside, transitional is visible; and (c) measured 4 mm from the outside, ferrite-pearlite is visible

4 Conclusions

The experimental results show that the scan speed has a direct correlation with the hardness response of S45C steel. The highest average surface hardness was obtained in Specimen 9 at 53.68 HRC with a speed of 3.66 mm/s, while Specimen 11 showed the best stability with an average of 53.00 HRC at a speed of 3.53 mm/s. An increase in scan speed up to 4.69-5.00 mm/s tends to decrease hardness. Meanwhile, its effect on the hardening depth shows the same tendency, where the highest hardness value is near the surface and decreases with increasing depth. The surface hardness is in the range of 446-637 HV, then decreases significantly at a depth of about 1–2.5 mm and eventually approaches the range of ±180-225 HV at deeper sections. High hardness near the surface can be attributed to rapid heating and cooling, resulting in a microstructure dominated by martensite. On the other hand, the decrease in hardness with depth indicates a reduction in the martensite fraction and an increase in ferrite and pearlite. The hard region consists of martensite, the transition region consists of ferrite and martensite, and the core section consists of ferrite and pearlite.

5 Acknowledgements

Pembiayaan dan Asesmen Pendidikan Tinggi (PPAPT), Ministry of Higher Education, Science, and Technology of the Republic of Indonesia for funding this research through the Doctoral Program Scholarship for Indonesian Lecturers, Fiscal Year 2025.

This paper was presented at the 12th International Conference and Exhibition on Sustainable Energy and Advanced Materials (ICE-SEAM 2026), held at Truntum Kuta, Bali, Indonesia, on 10-11 September 2026. It was subsequently submitted for consideration for publication in the Thematic section of the Journal of Applied Engineering Science associated with the conference. The paper was not published in the conference proceedings.

6 References

[1] Pfeifer, F., Knorr, L., Schlosser, F., Marten, T., & Tröster, T. (2023). Ecological and economic feasibility of inductive heating for sustainable press hardening processes. *Journal of Sustainable Development of Energy, Water and Environment Systems, 11(3)*, 1–20. https://doi.org/10.13044/j.sdewes.d11.0450

[2] Stević, Z., Dimitrijević, S. P., Stević, M., Stolić, P., Petrović, S. J., Radivojević, M., & Radovanović, I. (2023). The design of a system for the induction hardening of steels using simulation parameters. *Applied Sciences, 13(20),* Article 11432. https://doi.org/10.3390/app132011432

[3] Kombayev, K., Kim, A., Sypainova, G., & Yelemanov, D. (2023). Improving wear resistance by electrolyte-plasma hardening of corrosion-resistant steel of the tip. *Journal of Applied Engineering Science, 21(3)*, 810–819. https://doi.org/10.5937/jaes0-42291

[4] Al-Saraireh, F., & Suhymat, S. (2024). Effect of gas nitriding parameters on the micro-hardness of high-speed steel-cutting tools. *Journal of Applied Engineering Science, 22(3)*, 621–633. https://doi.org/10.5937/jaes0-50375

[5] Areitioaurtena, M., Segurajauregi, U., Fisk, M., Cabello, M. J., & Ukar, E. (2022). Numerical and experimental investigation on the residual stresses generated by scanning induction hardening. *Procedia CIRP, 108*, 827–832. https://doi.org/10.1016/j.procir.2022.03.127

[6] Holmberg, J., Wendel, J., & Stormvinter, A. (2024). Progressive induction hardening: Measurement and alteration of residual stresses. *Journal of Materials Engineering and Performance, 33(15),* 7770–7780. https://doi.org/10.1007/s11665-024-09703-0

[7] Šapek, A., Kalin, M., Godec, M., Donik, Č., & Markoli, B. (2024). Effect of feed rate during induction hardening on the hardening depth, microstructure, and wear properties of tool-grade steel work roll. *Journal of Materials Science: Materials in Engineering, 19(1),* Article 42. https://doi.org/10.1186/s40712-024-00193-5

[8] Saputro, I. E., Chiang, C.-P., Huang, H.-C., & Fuh, Y.-K. (2024). Origin of non-uniform tooth flank hardening distribution in SCM440 mobile induction heat-treated steel spur gears—A parametrical study with experimental–numerical coupled investigation. *The International Journal of Advanced Manufacturing Technology, 130(5–6),* 2915–2938. https://doi.org/10.1007/s00170-023-12859-z

[9] Li, H. P., Sun, Y., He, L. F., & Li, Z. C. (2023). Failure analysis of ball screw in the progressive induction hardening and finishing machining. *Engineering Failure Analysis, 151,* Article 107410. https://doi.org/10.1016/j.engfailanal.2023.107410

[10] Sun, Y., He, L., Gao, Y., Fang, S., Li, Z., & Li, H. (2024). Effect of induction quenching and tempering temperature on the mechanical properties and microstructure evolution of 45 steel for linear guide. *Journal of Materials Engineering and Performance, 33(22),* 12312–12321. https://doi.org/10.1007/s11665-023-08839-9

[11] Seo, E. J., Cho, L., De Moor, E., & Cryderman, R. L. (2025). Microstructural evolution during rapid induction heating and hardening of microalloyed 1045 medium carbon steels: Effect of initial microstructure. *Metallurgical and Materials Transactions A, 56(1),* 373–386. https://doi.org/10.1007/s11661-024-07649-5

[12] Holmberg, J., Hammersberg, P., Lundin, P., & Olavison, J. (2023). Predictive modeling of induction-hardened depth based on the Barkhausen noise signal. *Micromachines, 14(1),* Article 97. https://doi.org/10.3390/mi14010097

[13] Abdulhussein, H., Khalil, I., Ibrahim, R., Mohammed, M., & Alalwan, H. (2023). Protection of carbon steel from wear by quenching with nanotechnology to use it in dies parts. *Journal of Applied Engineering Science, 21(2),* 637–643. https://doi.org/10.5937/jaes0-41652

[14] Valentino, J., Pramono, A., Syaifudin, A., Kis, A., Shalahuddin, L., Windharto, A., & Sasaki, K. (2024). Enhancing S45C steel for the primary component of an automatic coupler using quench-tempering techniques. *Journal of Applied Engineering Science, 22(2)*, 215–222. https://doi.org/10.5937/jaes0-43988

[15] Hammouma, C., & Zeroug, H. (2022). Enhanced frequency adaptation approaches for series resonant inverter control under workpiece permeability effect for induction hardening applications. *Engineering Science and Technology, an International Journal, 27,* Article 101006. https://doi.org/10.1016/j.jestch.2021.05.010

[16] Choi, J., & Lee, S. (2020). High-frequency heat treatment of AISI 1045 specimens and current calculations of the induction heating coil using metal phase transformation simulations. *Metals, 10(11),* Article 1484. https://doi.org/10.3390/met10111484

[17] Taufik, A., Suprapto, A., & As'ad, S. (2018). Characteristic microstructure of micro hot rolled plate steel variating the radius of bending treatment with quenching and tempering heat treatment. *Journal of Applied Engineering Science, 16(4)*, 464–470. https://doi.org/10.5937/jaes16-18078

[18] Rudnev, V., Loveless, D., Cook, R. L., & Black, M. (2017). *Handbook of induction heating (2nd ed.)*. CRC Press.

[19] Nakasone, Y., Xiang, L., Mizobe, K., Matsueda, T., & Kida, K. (2023). Microstructure observation around hardness transition area of repeated induction heated S45C shaft. *Materials Science Forum, 1083,* 125–130. https://doi.org/10.4028/p-aqm1vv

[20] Gao, K., Wang, Z., Qin, X., & Zhu, S. (2016). Numerical analysis of 3D spot continual induction hardening on curved surface of AISI 1045 steel. *Journal of Central South University, 23(5),* 1152–1162. https://doi.org/10.1007/s11771-016-0365-8

7 Conflict of interest statement

The authors declare no conflict of interest.

8 Author contributions

Padang Yanuar: conceptualization, investigation, methodology, writing – original draft; Sri Nugroho: supervision, validation, writing – review & editing; Rifky Ismail: supervision, validation, conceptualization; Rizal Mustofa: investigation, formal analysis, visualization; Yanuar Mahfudz Safarudin: investigation, formal analysis, visualization.

9 Data availability statement

All relevant data has been included in this article.

10 Supplementary materials

There are no supplementary materials to include.

Paper submitted: 25.09.2026.
Paper accepted: 27.10.2026.
This is an open access article distributed under the CC BY 4.0 terms and conditions